Excitation Dynamics in Anisotropic Nanostructures of Star-Shaped CdS

Weon-Sik Chae,[†] Hee-Won Shin,[†] Eun-Seok Lee,[†] Eun-Jeong Shin,[†] Jin-Seung Jung,[‡] and Yong-Rok Kim*,[†]

Photon Applied Functional Molecule Research Laboratory, Department of Chemistry, Yonsei University, Seoul 120-749, and Department of Chemistry, Kangnung National University, Kangnung 210-702, South Korea

Received: December 9, 2004; In Final Form: February 7, 2005

Unique starlike CdS particles were prepared from the lyotropic triblock copolymer solution system. The starlike CdS consists of a spherical core and dozens of the attached conical nanolobes. From the comparative studies with the spherical and rod-shaped CdS nanoparticles, the unique photophysical property is presented for the starlike CdS particle. The experimental results suggest that the photogenerated charge carriers at the tip-edge region of the conical nanolobe in the starlike CdS system diffuse into the thicker inner part including the core region, which is possibly due to the decreasing excited state potential gradient from the tip edge to the thicker inner part. This type of charge carrier diffusion dynamics from the surrounding to the thicker inner part in this anisotropic morphology of the starlike CdS semiconductor closely resembles the energy transfer dynamics in the organic dendrimers.

1. Introduction

Two-dimensionally (2D) confined nanostructures (nanowires) have recently been much attracted as one of the interesting target materials in nanoscience because the nanowire can potentially be utilized as a building block for the integrated nanoconstructions such as nanocomplexes and nanodevices.[1−3] Since the degree of confinement in one direction is different from those in the other directions, the energetic properties of the anisotropic 2D confined nanostructures can be distinguished from those of the isotropic quantum dot systems. Such an anisotropic feature of the 2D confined nanostructures exhibits the distinctive optical and quantum transport properties.[4−7]

Recently, beyond the simple wire morphology, a variety of the anisotropic morphologies such as arrow, tear-drop, multipod, comblike, sea-urchin-like, and star shapes have been developed on the nanometer scale with the semiconductors under the controlled anisotropic growth conditions in aqueous solution and the gas phase.[8−10] Theoretical studies for the anisotropic semiconductor nanostructures revealed that the energetic properties dramatically depended on the factors of size and shape.[11,12] The lowest excited state is typically localized at the larger dimension of the anisotropic nanostructures, which can be expected from the quantum size effect: For a semiconductor with tetrapod morphology, the first electronic state is highly localized in the central region.[12] For another example of the heterojunctioned tetrapod semiconductor which consists of two or three types of the semiconductors with different band-gap energies, the photogenerated charge carriers can be populated either at the same region or a different space region depending on the junction type of the semiconductor nanostructure: The electrons and the holes are populated at the same region for the heterojunctioned type I semiconductor, whereas the electrons and the holes are localized at different space regions for the heterojunctioned type II semiconductor.[13]

For a star-shaped semiconductor quantum particle, one can envision that the band-gap potential increases from the inner thicker part to the tip edge of the quantum star particle due to the position-dependent gradual quantum size effect. In such anisotropic quantum particles, it is expected that the photophysical properties also depend on the position within the particle. In this study, we have investigated the photophysical properties of the prepared starlike CdS nanostructure compared with those of the spherical and rod-shaped CdS nanoparticles. This starlike CdS has a number of conical nanolobes attached to a spherical core. The conical nanolobe is of the unique 2D confined system which has the gradual change of the degree of confinement. In the single conical nanolobe, different confinement regimes coexist such as the strongly confined tip-edge region, the weakly confined inner thicker part, and the longest axis region which does not experience the confinement. For the starlike CdS, unprecedented photophysical properties, such as the gradual change of the band-gap potential within the anisotropic conical nanostructure and the pseudodendritic photodynamical diffusion, are observed in this anisotropic nanostructure.

2. Experimental Section

2.1. Sample Preparation. Triblock copolymers have recently been utilized for the preparation of various nanostructures such as nanoparticles, nanorods, and hollow nanospheres.[14−16] In this study, the triblock copolymer (Pluronic P123, $EO_{20}PO_{70}EO_{20}$) was utilized as a structure guiding assistant for the preparation of the novel starlike CdS nanostructure in the aqueous solution phase. To understand the structural and photophysical characteristics of the starlike CdS which consisted of the sphere and the conical nanolobes, the spherical and rod-shaped CdS particles were additionally synthesized from the aqueous and ethylenediamine (EDA) solutions of the Pluronic P123 at temperatures of 35 and 120 °C, respectively, for the comparative studies.

The synthetic procedure for the starlike CdS from the aqueous triblock copolymer solution is the following: 5.0 g of Pluronic

* Corresponding author. E-mail: yrkim@yonsei.ac.kr.
[†] Yonsei University.
[‡] Kangnung National University.

10.1021/jp044402v CCC: $30.25
Published on Web 03/11/2005

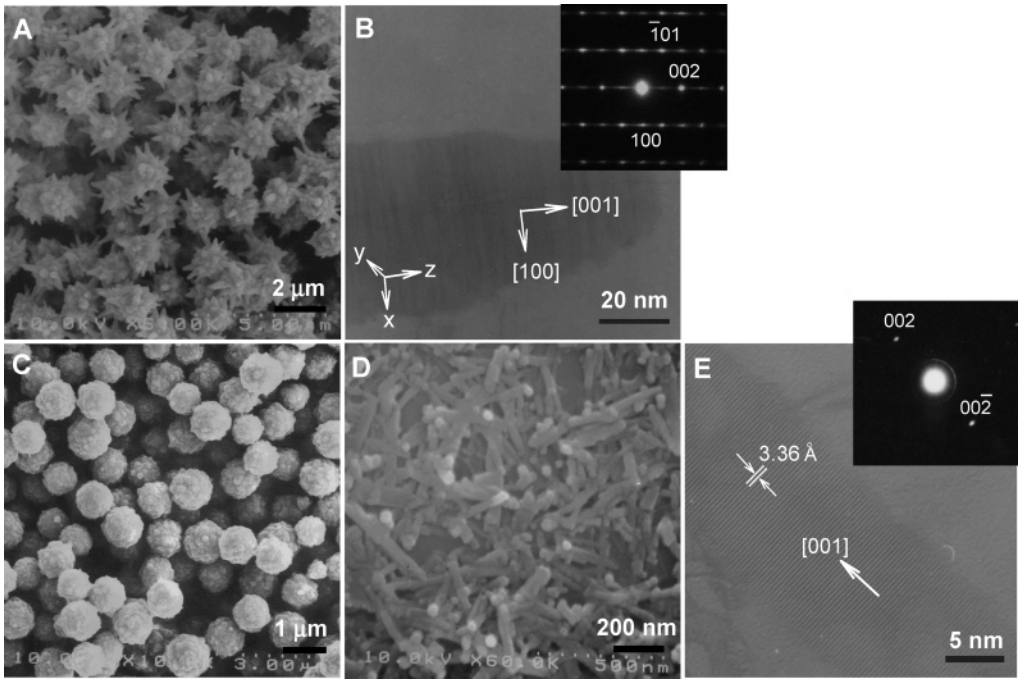

Figure 1. FE-SEM images for the (A) starlike, (C) spherical, and (D) rod-shaped CdS. TEM images of (B) the conical nanolobe of the starlike and (E) the rod-shaped CdS. The insets are SAED patterns of the conical nanolobe of the starlike and rod-shaped CdS.

P123 (purchased from Aldrich) and 1 mL of 15 M nitric acid were dissolved in 80 mL of distilled water. A 10 mL portion of an aqueous solution of 0.08 M $Cd(NO_3)_2 \cdot 4H_2O$ (purchased from Kanto Chemical in Japan) and 5 mL of an aqueous solution of 0.32 M thioacetamide (TAA, purchased from Acros) were added into the triblock copolymer solution and then homogeneously mixed. This mixture solution was maintained for 10 h at 80 °C without agitation, which gradually gave a pale yellow solution and changed to deep yellow and finally resulted in the orange-yellow powder which was precipitated in the bottom of the sealed reaction flask. Temperature was maintained at 80 ± 2 °C during the reaction.

Another reaction for the spherical CdS was conducted at 35 ± 2 °C with the same amounts of the chemicals utilized in the above reaction of the starlike CdS, which also produced the orange-yellow precipitate in the bottom of the sealed reaction flask. The other reaction for the rod-shaped CdS was conducted in the Teflon lined autoclave at 120 ± 2 °C with the same amounts of the chemicals utilized in the above reaction of the starlike CdS except for the solvent and the sulfur source. The EDA and the elementary sulfur were utilized as the solvent and the sulfur source, respectively, in the preparation of the rod-shaped CdS. This hydrothermal reaction produced the bright yellow precipitate in the bottom of the reaction vessel. All the precipitates were repeatedly washed with distilled water and ethanol to remove residual chemicals, and the resulting powder products were dried overnight in an oven at 50 °C.

2.2. Instrumentation. The powder precipitates from the reactions were subjected to field emission scanning electron microscope (FE-SEM, Hitachi S-4200), transmission electron microscope (TEM, JEOL 3011), powder X-ray diffraction (XRD, Mac Science M03XHF[22]) measurements. Absorption spectra were obtained from a diffuse reflectance UV−vis spectrophotometer (Jasco V-550) equipped with an integrating sphere (Jasco ISV-469). Steady state emission spectra were obtained from a spectrofluorometer (Hitachi F-4500). Temporal emission decays were obtained by utilizing a mode-locked Nd:YAG laser (Continuum Leopard-D10, full width at half-maximum (fwhm) of 23 ps, pulse energy of 50 μJ) and a streak camera system (Optronis Optoscope, temporal resolution of 2 ps). The laser system provides the instrumental response function (IRF) with a fwhm of ~23 ps which gives the detection limit of <5 ps from the iterative deconvolution process. All samples were excited at 315 nm which was generated with the Raman shifter pumped by the fourth harmonic pulse at 266 nm.

3. Results and Discussion

3.1. Structural Properties. The orange-yellow precipitate produced at 80 °C exhibits the novel starlike particles which consist of the core with a diameter of 1.3 ± 0.2 μm and the tens of conical nanolobes with a width of <200 nm in fwhm and the largest length of 600 nm (Figure 1A,B). The orange-yellow precipitate synthesized at 35 °C shows the spherical particles with a diameter of 0.85 ± 0.15 μm (Figure 1C), and the bright yellow solid products from the hydrothermal condition (120 °C) show the rod-shaped morphology with a width of 10−15 nm and a length of 300−500 nm (Figure 1D,E). All the products prepared from the triblock copolymer solutions show the narrow size distribution. TEM images and selected area electron diffraction (SAED) patterns for the conical nanolobe of the starlike and rod-shaped CdS present the characteristics of a highly crystalline hexagonal structure with a preferred growth direction of the [001] axis (Figure 1B,E).

For these interesting morphologies, X-ray diffraction patterns are presented in Figure 2. The strong diffractions of the spherical product show the well correlated pattern to the cubic phase β-CdS (JCPDS card no. 10-0454) with the Miller planes of (111), (220), and (311). The starlike product also presents the diffraction peaks for the cubic phase β-CdS as well as the additional weak diffraction peaks (marked with asterisks) which are closely matched with the Miller planes of (100), (101), and (103) for the wurtzite hexagonal phase CdS (JCPDS card no. 41-1049). On the basis of the TEM image and the electron diffraction pattern of the conical nanolobe, these newly observed hexagonal diffraction peaks can be assigned to the conical nanolobes that are attached to the cubic spherical core. For the rod-shaped product, the diffraction patterns are well matched

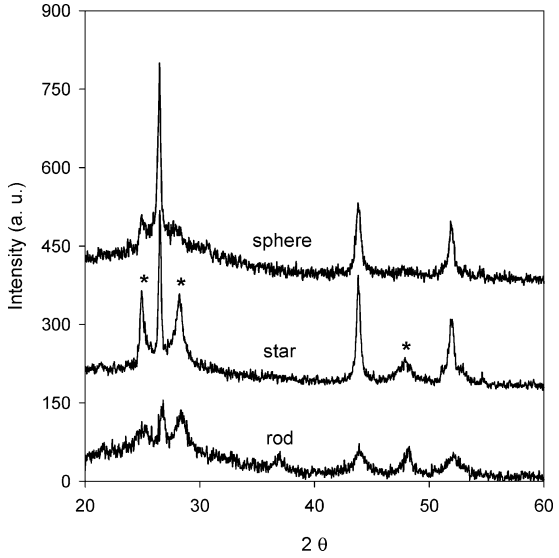

Figure 2. X-ray diffraction patterns for the (top) spherical, (middle) starlike, and (bottom) rod-shaped CdS.

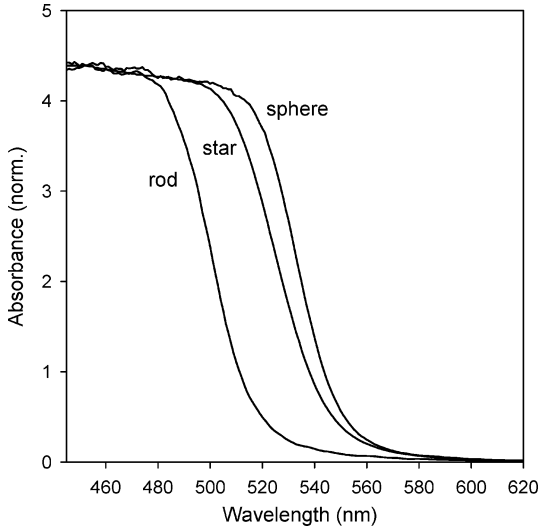

Figure 3. Absorption spectra for the spherical, starlike, and rod-shaped CdS at room temperature. The absorption spectra were obtained by applying the Kubelka−Munk function to the diffuse reflectance spectra.

with the wurtzite hexagonal phase CdS without the perceptible diffractions corresponding to the cubic phase CdS. The observed broadness of the diffraction peaks is due to the diffractional uncertainty which appears in nanometer sized particles.[17] On the other hand, the only diffraction peak at 26.8° in 2θ which corresponds to the (002) plane appears to be the narrow one. Such a narrow diffraction peak is due to the elongated anisotropic nanostructure of the rod-shaped CdS with a preferred growth direction of the [001] axis.[18]

Previously, the anisotropic nanostructures such as nanorods or nanowires were synthesized from aqueous solutions of the amphiphilic molecules utilized as structure assistants.[19,20] The similar formation mechanism possibly works for the formation of these nanostructures (starlike and rod) in the triblock copolymer aqueous solutions at temperatures of 80 and 120 °C, although there may exist somewhat complicated molecular interactions between the surfactant molecules and the inorganic precursors. Under these temperature conditions, because the liberation of H_2S from the decomposition of TAA which is a sulfur source is fast,[21] the crystal growth is expected to be dominated by the kinetic growth mechanism[9] which consequently results in an anisotropic crystal morphology with a preferred growth direction. However, this formation mechanism may not be effective at the low temperature (35 °C); since the liberation rate of the H_2S from TAA is so slow at 35 °C, the crystal growth can be determined by the decomposition rate of TAA[21] rather than by the anisotropic crystal growth rate of the CdS. Therefore, the isotropic morphology (spherical CdS) is to be produced at 35 °C.

The similar crystal growth behavior was also observed in the controlled condition of acidity for the formation of the CdS particles. The liberation rate of the H_2S from the TAA also depends on the acidity of the reaction solution: The high acidity increases the liberation rate of the H_2S from the TAA.[21] Under reduced acidic conditions, therefore, it is expected that the kinetic growth mechanism is not the favorable one for the formation of the CdS particle. As expected, the spherical morphology was observed from the reaction with the reduced acidity even at a reaction temperature of 80 °C (Supporting Information Figure S1). On the other hand, even at the relatively lower reaction temperature 35 °C, the anisotropic morphology of the flowerlike CdS was obtained from the reaction solution with the increased acidity (Supporting Information Figure S2). Therefore, the kinetic growth mechanism is responsible for the formation of the anisotropic morphologies of the CdS particles under the relatively high temperature and acidic conditions. Furthermore, since only spherical CdS was obtained from the acidic solution at 80 °C without the Pluronic P123 triblock copolymer (Supporting Information Figure S3), it was considered that the triblock copolymer molecules were also a contributing factor to the formation of the anisotropic CdS particles. In the case of the CdS nanorod under hydrothermal conditions, recent studies reported the importance of the chelation of monodentate, bidentate, and tridentate ligands for the anisotropic growth of nanostructures.[22,23] Therefore, it is considered that the chelating effect of the EDA molecules additionally assists the formation of the observed highly crystalline nanorod.

3.2. Optical Properties. The structure-dependent absorption spectra are presented in Figure 3. The absorption spectrum of the spherical CdS shows the absorption edge at ∼550 nm, which is similar to the spectral pattern of the bulk CdS (band-gap energy of 2.4 eV[24,25] at room temperature). The starlike CdS shows a slightly blue-shifted absorption spectrum from that of the spherical CdS, and the absorption spectrum for the rod-shaped CdS is further blue-shifted (Figure 3). Although the band gap of the bulk CdS with the hexagonal phase is known to be very similar to that of the cubic phase CdS,[26] the spectral blue-shifting is still observed from the cubic sphere to the hexagonal rod via the starlike structure. It implies that the observed spectral shift is due to the confinement effect of the photoexcited carriers (electrons and holes). Since the widths of the conical nanolobes and nanorods of the synthesized CdS are larger than the exciton Bohr diameter of the bulk CdS (48−58 Å),[27,28] the spatial confinement effect for the photoexcited carriers is expected to be weak.[28] Therefore, only the slight spectral blue-shift which is not more than ∼30 nm (∼0.14 eV) is observed. Furthermore, it is noteworthy that the starlike CdS shows the gradually rising blue-shift of the absorption compared with that of the spherical CdS, while the band-edge absorptions are similar in both the structures. Such spectral characteristics of the starlike CdS suggest the existence of the unique band-gap potential which gradually increases as the potential dimension changes from the core region to the tip edge of the conical nanolobes.

From the steady state emission spectra for the series of the CdS nanostructures, it is observed that the emission bands are

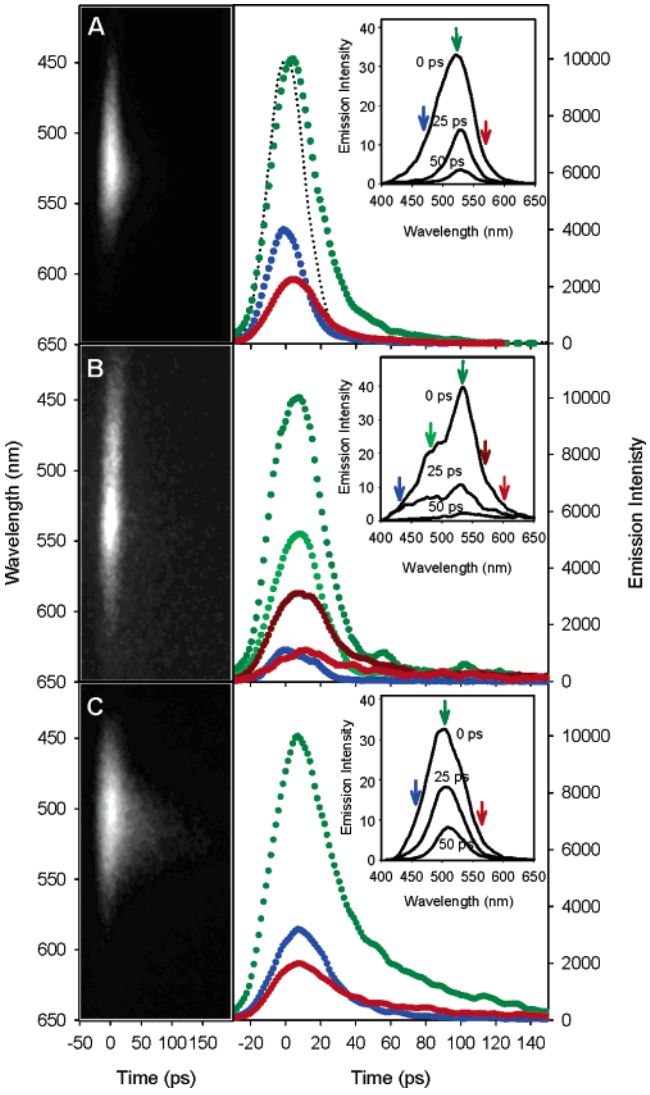

Figure 4. Picosecond time-resolved emission decays for the (A) spherical, (B) starlike, and (C) rod-shaped CdS particles at room temperature. (left) Two-dimensional images from streak camera are shown in time and wavelength. (right) The time-resolved emission decays are presented at the selected wavelengths, as indicated by the color arrows in the corresponding emission spectra. The insets show the selected emission spectra detected at three transient times of 0, 25, and 50 ps. All emission decays for the CdS particles are distinguishable from the instrumental response function (IRF) with a fwhm value of ~23 ps, which is presented as a black dotted line.

dominantly located at a shorter wavelength region than 600 nm (Supporting Information Figure S4). The previous reports assigned the similar band-edge emission to the direct exciton recombination and/or the shallowly trapped exciton recombination for CdS.[29,30] The emission originating from the surface trap states, which are typically ranged in the spectral region 600−800 nm,[30,31] also appears in a weak intensity. However, the laser induced time-resolved emission spectra show the core state emissions which are dominantly located near the band gap, while the surface state emission is not prominent in the spectral region 600−670 nm within a time window of 400 ps (Figure 4 and Supporting Information Figure S4). Such suppressed surface state emissions in the laser induced time-resolved emission spectra are possibly ascribed to the high photon intensity of the laser excitation source compared with the low intensity of the Xe-lamp excitation source utilized for the steady state emission. With the high intensity of laser excitation, it was reported that the deeply trapped emission state such as the surface electronic state could easily be saturated and, therefore, the emissions from the direct and/or shallowly trapped states would be dominantly appeared,[31,32] similar to the results of the time-resolved emissions in this study.

TABLE 1: Lifetime Components for the Emission Decays of the CdS Nanostructures at Room Temperature[a]

sample	λ_{det} (nm)	rise (ps)	mean lifetime ($\langle\tau\rangle$) (ps)
spherical CdS	470		<5
	530		15
	570		15
starlike CdS	430		6
	480		12
	530		20
	570	~5	40
	600	~5	75
rod-shaped CdS	450		18
	530		38
	570		59

[a] The recombination decays consist of the multiple lifetime components due to the diverse recombination paths; therefore, the recombination lifetime is simply shown as the mean lifetime ($\langle\tau\rangle$). The mean lifetime is deduced as follows: $\langle\tau\rangle = \sum_i A_i\tau_i^2/\sum_i A_i\tau_i$, in which the parameters are estimated from iterative least-squares deconvolution fitting of the emission decays with the expression $I(t) = A_1e^{-t/\tau_1} + A_2e^{-t/\tau_2} + ...$; $I(t)$ is the time-dependent emission intensity, A is the amplitude, and τ is the lifetime.

From the time-resolved emissions, as the particle dimension decreases from the spherical to rod-shaped CdS, the emission spectrum is shifted as much as ~20 nm to the short wavelength region (Figure 4). The spectrum for the starlike CdS interestingly appears to be the convoluted one of the emission spectra of the spherical and rod-shaped CdS. For these CdS particles, the emission spectra observed at room temperature show a somewhat broad pattern with a fwhm of 0.35−0.45 eV. Such broad spectra are possibly attributed to the various recombination paths for the photogenerated carriers in the CdS,[33] the size distributions, and the convoluted spectrum in the case of the starlike CdS. Therefore, it is typically expected that they have the broad distribution of the lifetimes depending on the respective emission states. Therefore, as shown in Table 1, the distributed lifetimes are presented to be the mean lifetimes depending on the different detection wavelengths (λ_{det}). The interesting point is that the rod-shaped CdS shows relatively longer recombination lifetimes than those observed in the spherical one. There can be two possible origins for the recombination rate change in a reduced size of semiconductor nanostructure: One is the increased recombination rate (shorter lifetime) which is due to the enhanced coupling between the spatially confined charge carriers (electron and hole) in a strongly confined system,[34,35] and the other is the decreased recombination rate (longer lifetime) which is caused by the reduced phonon coupling to the quantized electronic states.[36−38] Therefore, the decreased recombination rate (longer lifetime) observed in the CdS nanorod is plausibly ascribed to the reduced optical phonon coupling during the carriers' recombination processes.

For the novel starlike CdS complex which consists of the spherical core and the attached conical nanolobes, an intense peak centered at ~530 nm with a shoulder at ~480 nm is observed. Since the intense peak and the left shoulder are similarly positioned with the respective emissions of the spherical and rod-shaped CdS, it may be proposed that the intense center and the left-shoulder emissions are attributed to the spherical core and the conical nanolobes of the starlike CdS, respectively. Since the left-shoulder emission originates from the recombination processes within the conical nanolobes of

the starlike CdS, a longer recombination lifetime is expected for the left-shoulder emission due to the less optical phonon coupling, compared with the emission lifetime detected at the intense center emission band which originates from the emission states in the spherical core. However, contrary to this expectation, the observed recombination lifetimes 6 and 12 ps for the left-shoulder emissions at 430 and 480 nm are shorter than the lifetime 20 ps for the intensive center emission at 520 nm. Such an unexpected result implies that the carriers' relaxation dynamics within the conical nanolobes seems to experience the other pathway rather than the optical phonon coupled recombination process. As the possible dynamics, it can be suggested that the diffusion of the photoexcited charge carriers (electron and hole) occurs from the tip edge of the conical nanolobes to the thicker inner part including the core of the starlike CdS.

For this unique 2D confined nanostructure of the conical nanolobe, the quantum size effect provides the qualitative picture for the band-gap potential. The conical shape has a more complicated feature of the confinement effect than the cases of the simple quantum dots and rods. On the basis of the quantum size effect, it is expected that the band-gap potential is varied with the vector directions in the conical nanolobe: The potential band gap in the lateral dimension (*x*,*y*-directions, as shown in Figure 1B) around the nanolobe axis gradually increases with decreasing lateral dimension, of which the potential band gap has the highest value at the tip edge, while the longer axis (*z*-direction, as shown in Figure 1B) along the conical nanolobe has a somewhat insensitive potential energy gap. Such different degrees of the confinement in the starlike CdS are the reasons for the gradual rise in the absorption spectrum toward that of the hexagonal nanolobe. Therefore, the charge carriers' diffusion can be realized in the decreasing band-gap potential gradient with the change of the lateral dimension from the tip edge to the thicker inner part of the attached conical nanolobe including the core part of the starlike CdS.

Such charge carriers' diffusion within the unique conical nanolobe of the starlike CdS is additionally supported by the other results: The rise component of ~5 ps is detected in the lifetime decays at 570 and 600 nm. Moreover, the recombination lifetimes in the thicker inner region including the core part of the starlike CdS show slower recombination lifetimes of 20, 40, and 75 ps than that (15 ps) of the spherical CdS even though the averaged inner core dimension of the starlike CdS particle (>1 μm) is larger than the diameter of the spherical CdS (<1 μm). This type of carrier diffusion from the outer surrounding part to the thicker inner part including the core along the decreasing band-gap potential closely mimics the unique feature of the energy transfer which is typically observed in organic dendrimers.[39] Therefore, this novel structure of the starlike CdS would be applied for the light-harvesting system as a new type of inorganic dendrimer.

As the charge carriers diffuse and possibly trap into the thicker inner part including the core by following the decreased gradient of the excited state potential surface, the diffusion rate of the charge carriers in the solid state CdS can be estimated approximately by applying the effective masses to the conventional simple model for the carriers' mobility: The carriers' mobility is inversely proportional to the effective masses of the charge carriers.[40] Since the hole mass (0.80−0.98 m_0*) is heavier than the electron mass (0.17−0.19 m_0*) by 4−5 times,[41,42] it can be considered that the diffusion rate of the photoexcited electrons in the gradient potential is relatively faster than that of the holes. In a simple picture, the carriers' retention time at the tip-edge region of the conical nanolobe is expected to be much longer for the photoexcited holes than that for the photoexcited electrons. In the starlike CdS system, therefore, the temporal density gradient map seems to exist for the photogenerated charge carriers between the tip-edge part of the conical nanolobe and the thicker inner part including the core of the starlike CdS right after the photon irradiation: In respect of the transient dynamics, it is carefully suggested that the photogenerated electrons can be more easily found at the inner part of the larger dimension and the smaller band-gap energy, whereas the photogenerated holes can be found more at the tip edge of the conical nanolobe of the smaller dimension and the larger band-gap energy.

4. Conclusions

In summary, we have investigated the photophysical properties of the newly synthesized starlike CdS, which was prepared from the lyotropic triblock copolymer solution. The starlike CdS shows the photogenerated charge carriers' diffusion from the tip edge of the conical nanolobes to the thicker inner part including the core, likely as the light-harvesting system of the organic dendrimer. Furthermore, it is expected that the photoexcited holes are more populated at the tip-edge region during the light irradiation due to the expected mobility difference between the holes and the electrons over the gradient potential surface which depends on the quantum nanostructure. These unique features of the charge carriers' diffusion and the temporal density gradient in the designed anisotropic semiconductor nanostructure may provide an intuitive protocol for further understanding and development of the complicated nanomaterials and nano-biological systems.

Acknowledgment. This work was financially supported by a National Research Laboratory (Grant No. M1-0302-00-0027) program administered by the Ministry of Science and Technology (MOST). We are grateful for instrumental support from the equipment facility of CRM-KOSEF, Korea University. Prof. J.-S. Jung thanks for a grant, Myongji RRC.

Supporting Information Available: FE-SEM images of the various CdS particles prepared from the various conditions of acidity, temperature, and triblock copolymer and steady state and laser induced time-resolved emission spectra of the series of the CdS nanostructures. This material is available free of charge via the Internet at http://pubs.acs.org.

References and Notes

(1) Huang, M. H.; Mao, S.; Feick, H.; Yan, H.; Wu, Y.; Kind, H.; Weber, E.; Russo, R.; Yang, P. *Science* **2001**, *292*, 1897.
(2) Melosh, N. A.; Boukai, A.; Diana, F.; Gerardot, B.; Badolato, A.; Petroff, P. M.; Heath, J. R. *Science* **2003**, *300*, 112.
(3) Zhong, Z.; Wang, D.; Cui, Y.; Bockrath, M. W.; Lieber, C. M. *Science* **2003**, *302*, 1377.
(4) Hu, J.; Li, L.-S.; Yang, W.; Manna, L.; Wang, L.-W.; Alivisatos, A. P. *Science* **2001**, *292*, 2060.
(5) Katz, D.; Wizansky, T.; Millo, O.; Rothenberg, E.; Mokari, T.; Banin, U. *Phys. Rev. Lett.* **2002**, *89*, 086801.
(6) Ma, D. D. D.; Lee, C. S.; Au, F. C. K.; Tong, S. Y.; Lee, S. T. *Science* **2003**, *299*, 1874.
(7) Barrelet, C. J.; Greytak, A. B.; Lieber, C. M. *Nano Lett.* **2004**, *4*, 1981.
(8) Manna, L.; Scher, E. C.; Alivisatos, A. P. *J. Am. Chem. Soc.* **2000**, *122*, 12700.
(9) Lee, S.-M.; Jun, Y.; Cho, S.-N.; Cheon, J. *J. Am. Chem. Soc.* **2002**, *124*, 11244.
(10) Yan, H.; He, R.; Johnson, J.; Law, M.; Saykally, R. J.; Yang, P. *J. Am. Chem. Soc.* **2003**, *125*, 4728.
(11) Hu, J.; Wang, L.-W.; Li, L.-S.; Yang, W.; Alivisatos, A. P. *J. Phys. Chem. B* **2002**, *106*, 2447.
(12) Li, J.; Wang, L.-W. *Nano Lett.* **2003**, *3*, 1357.

(13) Milliron, D. J.; Hughes, S. M.; Cui, Y.; Manna, L.; Li, J.; Wang, L.-W.; Alivisatos, A. P. *Nature* **2004**, *430*, 190.
(14) Yang, C.-S.; Awschalom, D. D.; Stucky, G. D. *Chem. Mater*. **2002**, *14*, 1277.
(15) Bao, N.; Shen, L.; Lu, X.; Yanagisawa, K.; Feng, X. *Chem. Phys. Lett*. **2003**, *377*, 119.
(16) Ma, Y.; Qi, L.; Ma, J.; Cheng, H.; Shen, W. *Langmuir* **2003**, *19*, 9079.
(17) Klug, H. P.; Alexander, L. E. *X-ray Diffraction Properties for Polycrystalline and Amorphous Materials*; Wiley: New York, 1974.
(18) Routkevitch, D.; Bigioni, T.; Moskovits, M.; Xu, J. M. *J. Phys. Chem*. **1996**, *100*, 14037.
(19) Murphy, C. J.; Jana, N. R. *Adv. Mater*. **2002**, *14*, 80.
(20) Liu, Z.; Hu, Z.; Xie, Q.; Yang, B.; Wu, J.; Qian, Y. *J. Mater. Chem*. **2003**, *13*, 159.
(21) Yamaguchi, K.; Yoshida, T.; Sugiura, T.; Minoura, H. *J. Phys. Chem. B* **1998**, *102*, 9677.
(22) Li, Y.-D.; Liao, H.-W.; Ding, Y.; Qian, Y.-T.; Yang, L.; Zhou, G.-E. *Chem. Mater*. **1998**, *10*, 2301.
(23) Yang, J.; Xue, C.; Yu, S.-H.; Zeng, J.-H.; Qian, Y.-T. *Angew. Chem., Int. Ed*. **2002**, *41*, 4697.
(24) Rossetti, R.; Hull, R.; Gibson, J. M.; Brus, L. E. *J. Chem. Phys*. **1985**, *82*, 552.
(25) Nosaka, Y. *J. Phys. Chem*. **1991**, *95*, 5054.
(26) Ramakrishna, M. V.; Friesner, R. A. *J. Chem. Phys*. **1991**, *95*, 8309.
(27) Zhang, J. Z. *Acc. Chem. Res*. **1997**, *30*, 423.
(28) Kayanuma, Y. *Phys. Rev. B* **1988**, *38*, 9797.
(29) O'Neil, M.; Marohn, J.; McLendon, G. *J. Phys. Chem*. **1990**, *94*, 4356.
(30) Chae, W.-S.; Ko, J.-H.; Hwang, I.-W.; Kim, Y.-R. *Chem. Phys. Lett*. **2002**, *365*, 49.
(31) Wu, F.; Zhang, J. Z.; Kho, R.; Mehra, R. K. *Chem. Phys. Lett*. **2000**, *330*, 237.
(32) Kang, S.-G.; Chae, W.-S.; Kim, Y.-R.; Jung, J.-S.; Lee, S.-H. *Chem. Phys*. **2000**, *256*, 295.
(33) Gaponenko, S. V. *Optical Properties of Semiconductor Nanocrystals*; Cambridge University Press: New York, 1998.
(34) Bockelmann, U.; Egeler T. *Phys. Rev. B* **1992**, *46*, 15574.
(35) Efros, A. L.; Kharchenko, V. A.; Rosen, M. *Solid State Commun*. **1995**, *93*, 281.
(36) Benisty, H. *Phys. Rev. B* **1995**, *51*, 13281.
(37) Alivisatos, A. P.; Harris, T. D.; Carroll, P. J.; Steigerwald, M. L.; Brus, L. E. *J. Chem. Phys*. **1989**, *90*, 3463.
(38) Ramvall, P.; Tanaka, S.; Nomura, S.; Riblet, P.; Aoyagi, Y. *Appl. Phys. Lett*. **1999**, *75*, 1935.
(39) Adronov, A.; Fréchet, J. M. J. *Chem. Commun*. **2000**, 1701.
(40) Yu, P. Y.; Cardona, M. *Fundamentals of Semiconductors*; Springer: New York, 2001.
(41) Vossmeyer, T.; Katsikas, L.; Giersig, M.; Popovic, I. G.; Diesner, K.; Chemseddine, A.; Eychmüller, A.; Weller, H. *J. Phys. Chem*. **1994**, *98*, 7665.
(42) Wang, Y.; Suna, A.; McHugh J.; Hilinski, E. F.; Lucas, P. A.; Johnson, R. D. *J. Chem. Phys*. **1990**, *92*, 6927.